

Atomic-Scale Molecular Dynamics Simulations of DNA–Polycation Complexes: Two Distinct Binding Patterns

Diana A. Kondinskaia,[†] Andrei Yu. Kostritskii,[†] Alexey M. Nesterenko,[‡] Alexandra Yu. Antipina,[†] and Andrey A. Gurtovenko^{*,†,§}

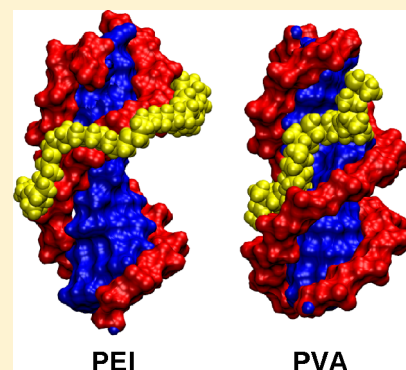
[†]Faculty of Physics, St. Petersburg State University, Ulyanovskaya str. 3, Petrodvorets, St. Petersburg 198504, Russia

[‡]Belozersky Institute of Physico-Chemical Biology, Lomonosov Moscow State University, Leninskie Gory, 1/40, Moscow 119991, Russia

[§]Institute of Macromolecular Compounds, Russian Academy of Sciences, Bolshoi Prospect V.O. 31, St. Petersburg 199004, Russia

Supporting Information

ABSTRACT: Synthetic cationic polymers represent a promising class of delivery vectors for gene therapy. Here, we employ atomistic molecular dynamics simulations to gain insight into the structure and properties of complexes of DNA with four linear polycations: polyethylenimine (PEI), poly-L-lysine (PLL), polyvinylamine (PVA), and polyallylamine (PAA). These polycations differ in their polymer geometries, protonation states, and hydrophobicities of their backbone chains. Overall, our results demonstrate for the first time the existence of two distinct patterns of binding of DNA with polycations. For PEI, PLL, and PAA, the complex is stabilized by the electrostatic attraction between protonated amine groups of the polycation and phosphate groups of DNA. In contrast, PVA demonstrates an alternative binding pattern as it gets embedded into the DNA major groove. It is likely that both the polymer topology and affinity of the backbone chain of PVA to the DNA groove are responsible for such behavior. The differences in binding patterns can have important biomedical implications: embedding PVA into a DNA groove makes it less sensitive to changes in the aqueous environment (pH level, ionic strength, etc.) and could therefore hinder the intracellular release of genetic material from a delivery vector, leading to lower transfection activity.



INTRODUCTION

Interactions of synthetic cationic polymers with nucleic acids have been of tremendous interest during the past few decades as these polymers represent a promising class of delivery vectors for gene therapy.¹ In particular, cationic polymers are efficient in condensing polyanionic DNA/RNA molecules; hence, they are considered as a reasonable alternative to viral delivery agents² (the latter are often characterized by both high cytotoxicity and immunogenicity).³ Furthermore, synthetic polycations, being of relatively low production cost, can easily be designed and tuned to have a specific structure and charge distribution.^{1,4}

Historically, linear poly-L-lysine (PLL) and polyethylenimine (PEI) are among the most studied polycations used as gene-delivery vectors.⁵ Interactions of PLL with nucleic acids were studied for the first time in ref 6, with the aim of better understanding gene expression, as some histones are enriched with lysine. An additional advantage of PLL is that it is biodegradable, as its backbone has a polypeptide structure. Because of the relatively low transfection efficiency of pure PLL, several block copolymers of PLL with polyethyleneglycol⁷ and chitosan⁸ have recently been explored to improve its transfection properties. As far as PEI is concerned, the polymer is often considered one of the most efficient polycation

transfection agents.⁹ Numerous experimental studies have addressed several important aspects of PEI-based delivery vectors. In particular, the impact of molecular weight¹⁰ and polymer architecture¹¹ (linear vs branched topology) on transfection efficiency and cytotoxicity has been considered. Similar to PLL, several modifications of PEI have been studied, including copolymers of PEI with polyethyleneglycol¹² and uronic acid¹³ as well as peptide-conjugated PEI-based polymers.¹⁴ Despite the modifications, both pure PLL and PEI are often considered important reference polycations for gene delivery.¹

In addition to experimental studies, atomistic computer simulations have recently been employed to gain insight into the structure and properties of DNA/RNA–polycation complexes.¹⁵ Following pioneering simulation studies of interactions of DNA with short polyamines,^{16,17} most computational efforts have been focused by far on complexes of nucleic acids with PLL^{18–23} and PEI.^{18,23–25} Overall, it was shown that the formation of complexes with DNA/RNA followed the same pattern for both PLL and PEI: the

Received: April 13, 2016

Revised: June 8, 2016

Published: June 9, 2016

complexation was mainly driven by the electrostatic attraction between protonated amine groups of the polymer and negatively charged phosphate groups of the DNA molecule.^{18,24}

Furthermore, both PLL and PEI showed some (weaker) interactions with electronegative atoms of DNA grooves. On the other hand, PEI, being more flexible compared to PLL, demonstrated more effective neutralization of DNA charges.¹⁸ Most recently, Sammalkorpi et al. reported computational studies on DNA–polycation decomplexation through the addition of salt to the polyelectrolyte system (divalent CaCl_2 salt was shown to be significantly more effective than its monovalent counterpart).^{22,23}

It is noteworthy that both PLL and PEI have amine groups in their backbone chains, which make them hydrophilic even if the amines are not protonated. Besides PLL and PEI, other types of polycations have also been synthesized and explored with respect to their transfection properties. In particular, polyvinylamine (PVA) and polyallylamine (PAA), two linear polymers with short side chains bearing cationic residues, were examined;²⁶ see Figure 1 for the chemical structures of the

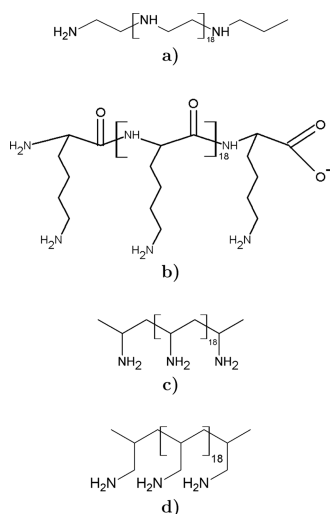


Figure 1. Chemical structures of the polycations used for complexation with DNA: (a) PEI, (b) PLL, (c) PVA, and (d) PAA. The polymers in fully deprotonated states are shown.

polymers. It was demonstrated that both PVA and PAA were efficient in the formation of stable complexes with DNA as well as in charge neutralization of polynucleotides.²⁶ A markedly high transfection efficiency was observed in the case of PAA.²⁷ Both PVA and PAA have a hydrocarbon backbone chain, which makes them different from PLL and PEI as far as the hydrophobicity of the main chain is concerned. Therefore, one can expect that the microscopic structure and properties of DNA–polycation complexes could differ for these two classes of cationic polymers. The possible differences can be unlocked, for example, with the use of computer modeling along with models of high resolution. However, to the best of our knowledge, no computer simulation studies have been reported so far for polycations with hydrocarbon backbone chains, such as PVA and PAA.

To compensate for the lack of such studies, in this work we employ atomic-scale molecular dynamics (MD) simulations to gain insight into the structure and properties of complexes of DNA with cationic polymers that have different types of backbone chains. In particular, complexes of DNA with four

polycations (PLL, PEI, PVA, and PAA) were studied and systematically compared. The use of long MD simulations (up to 1 μs) allowed us to distinguish two binding patterns in DNA–polycation complexes. In addition to the previously observed binding due to the electrostatic attraction between the cationic residues of the polymers and phosphate groups of DNA, we found that polymers with a hydrocarbon backbone chain (PVA) can also get embedded into the major groove of DNA.

METHODS

We have performed atomic-scale MD simulations of a short double helix of DNA with four different cationic polymers: PEI, PLL, PVA, and PAA; see Figure 1 for the chemical structures of the polymers. Each simulated system consisted of a DNA fragment and a polymer chain. A widely studied Dickerson dodecamer^{28,29} ($\text{d}(\text{CGCGAATTCGCG})_2$, 12 base pairs, total charge of $-22e$) was chosen as the DNA fragment; see Figure S1 for the numbering of atoms of DNA bases. The initial configuration of DNA was taken from ref 30. Each cationic polymer consisted of 20 monomer units. Because of the current limitations of computational models of high resolution, the DNA fragment and polymers are much shorter than those considered in experiment. Such small molecules are well suited for studying atomic-scale details of DNA–polycation interactions, although some care should be taken to eliminate possible end effects.

A DNA–polycation system was solvated in water, and the number of water molecules varied from $\sim 11\,000$ (PEI and PVA) to $\sim 16\,500$ (PLL and PAA). An appropriate number of DNA and polycation counterions (Na^+ and Cl^- ions) was added to the systems to achieve electroneutrality. The total number of atoms amounted to $\sim 34\,000$ for PEI and PVA systems and $\sim 51\,000$ for PLL and PAA systems; see Table 1 for details.

The protonation state of polycations depends on the pH of the aqueous solution. As classical MD simulations are not suited to control pH, the pH level has to be fixed before the

Table 1. Simulated DNA–Polycation Systems

polycation	run number	simulation time [ns]	number of atoms
PEI	1	1000	34 046
	2	800	34 075
	3	400	34 037
	4	400	34 085
PVA	1	800	34 076
	2	400	34 109
	3	200	34 109
PLL	1	500	51 223
	2	300	51 196
	3	300	51 211
PAA ^a	1	700	51 260
	2	500	51 281
	3	200	51 257
PAA (50%) ^b	1	500	51 242
	2	250	51 239
	3	250	51 254
PEI-Ca ^c	1	700	32 858
PVA-Ca ^c	1	700	32 888

^a20%-protonated PAA. ^b50%-protonated PAA. ^cA DNA–polycation system with 1 M CaCl_2 .

beginning of the simulations. In particular, this implies that our simulations are not able to address the possible changes in protonation upon formation of a DNA–polycation complex. In this work, we chose to consider physiologic conditions (pH 7). Under these conditions, each monomer unit of PLL is protonated, whereas the protonation level of PEI is close to 50% (every other monomer is protonated).^{31,32} As far as the protonation level of polymers with hydrocarbon backbone chains is concerned, it is 50% for PVA³³ and 20% for PAA.³¹ The distribution of protonated and deprotonated monomers for all four polymers is shown in Figure S2. Furthermore, for the sake of comparison with PEI and PVA systems, we also performed simulations with 50%-protonated PAA; see Table 1. Therefore, the polymers differ not only in their chemical structures but also in their protonation states.

DNA was described in the framework of the AMBER parmbsc0 force field,³⁴ whereas the AMBER99 force field³⁵ was used for all cationic polymers. Partial charges for PLL were taken from the AMBER99 force field. Water was represented by the TIP3P model.³⁶ As standard AMBER force-field parameters for monovalent ions (Na^+ and Cl^-) are known to give rise to serious artifacts, we chose to use an improved set of ion parameters, developed in ref 37. For Ca^{2+} ions we used standard AMBER parameters.

The partial charges of PEI, PVA, and PAA were obtained using ab initio calculations, according to the following protocol. Four trimers were constructed from protonated (“P”) and deprotonated (“D”) monomers: DDD, DPD, PDP, and PPP. The geometry of each trimer was first optimized with RDFT(B3LYP5) in the SBKJC basis set with an effective core potential;³⁸ the basis set was then extended to 6-31G(1p,1d). The Firefly software (version 8) was used for all ab initio calculations.³⁹ The electrostatic potential was computed in the 6-31G(1p,1d) basis set with the MP2 theory level at a Connolly surface near each trimer in its optimized geometry. Such an approach is recommended for parameterization of the AMBER force field.⁴⁰ Finally, partial charges were fit to reproduce the ab initio electrostatic potential; the RESP algorithm⁴¹ was used for fitting. All partial charges of PEI, PVA, and PAA are listed in the Supporting Information.

The systems were simulated in the NPT ensemble at $P = 1$ bar and $T = 300$ K. A velocity-rescaling thermostat was used to control the temperature.⁴² The pressure was kept constant using an isotropic Parrinello–Rahman barostat.⁴³ The particle-mesh Ewald method was used for handling electrostatic interactions.⁴⁴ A cutoff of 1 nm was set for Lennard–Jones interactions. The time step was 2 fs. The Gromacs 4.5.6 suite was used in all simulations.⁴⁵

Before actual simulations of the DNA–polycation systems, the DNA fragment and polycations were well equilibrated separately in aqueous solution. These simulations provided us with a number of pre-equilibrated samples of DNA and polymers, which were taken for building up the initial configurations of complexes. The initial distance between a DNA fragment and polycation was set to 1 nm (the distance was measured between the closest DNA and polymer atoms). Each production run is preceded by energy minimization, and a short run with position restraints applied to both DNA and the polymer.

To improve the statistical reliability of the results, MD simulations of DNA–polycation complexes were repeated independently several times for each polycation. Simulations of DNA–PEI systems were repeated four times, whereas

simulations of complexes of DNA with the rest of the polycations were repeated three times for each polymer; the simulation time of individual runs varied from 200 ns to 1 μs ; see Table 1. Furthermore, we used different samples of DNA and polycations to make individual runs statistically independent. Throughout the paper, we chose to present the results for only one system per polycation, namely, for PEI-1, PVA-1, PAA-2, and PLL-1 systems. Most of the results (unless stated otherwise) hold for the rest of the simulation runs for a particular DNA–polycation system, with the exception of some end effects, which are considered artifacts.

To complement our study, we also performed two additional simulations of complexes of DNA with PEI and PVA in the presence of 1 M CaCl_2 salt; see Table 1. As starting configurations, two stable complexes were chosen (the PEI-1 system at $t = 1 \mu\text{s}$ and PVA-1 system at $t = 650$ ns). Simulations of the systems with CaCl_2 salt were 700 ns long.

RESULTS

Kinetics of DNA–Polycation Complex Formation. The four types of polycations considered in this work differ in both polymer geometry (see Figure 1) and protonation level. As all of the polymers consist of 20 monomer units, differences in their protonation can directly be related to the overall charge of the polycations. The total charges of PLL and PAA amount to $+20e$ and $+4e$, respectively. In turn, PEI and PVA, with the same protonation level of 50%, carry an overall charge of $+10e$ each. Given that the total charge of a DNA dodecamer is $-22e$, for all four polymers, one can expect electrostatically driven formation of a DNA–polycation complex. As seen from the time evolution of the distances between the centers of masses (COMs) of a DNA fragment and polymer, this is indeed the case (see Figure 2).

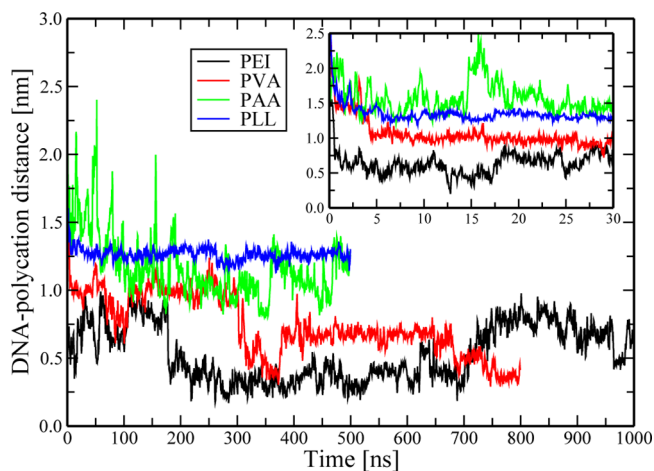


Figure 2. Time evolution of the distances between the COMs of a DNA fragment and polymer. Results for the PEI-1 (black line), PVA-1 (red line), PAA-2 (green line), and PLL-1 (blue line) systems are shown. The inset shows initial 30 ns long parts of MD trajectories.

Interestingly, the initial formation of a DNA–polycation complex is a relatively fast process. The complexation rate can directly be related to the overall charge of the polycation. In particular, it takes only ~ 2 ns for a highly charged PLL to form a complex with DNA, whereas for PAA (a polycation with the lowest charge), the time required for initial complexation exceeds 20 ns; see Figure 2 (inset). PEI and PVA form

complexes with DNA within ~ 5 ns; that is, they show an intermediate behavior in line with the value of their total charge. We note that these complexation times will depend on the initial distance between DNA and the polycation; hence, they should be used only for the sake of comparison of the relative complexation rates for different polymers.

Overall, the time evolution of the distances between the COMs of DNA and a polycation allows us to unlock some basic features of the complexation process. In particular, PLL forms the most stable complex with DNA in terms of fluctuations of its COM with respect to the COM of DNA; see Figure 2. This is most likely due to the very large positive charge of PLL. In contrast, the corresponding characteristics measured for PAA, the polymer with the smallest charge, exhibit very large fluctuations. Visual inspection shows that binding of PAA to DNA is rather weak and unstable. Although complete decomplexation is not observed, one can witness the states when a polymer is bound to DNA by only one chain end; this seems to be typical for the initial part of the trajectory. Additionally, the large fluctuations are linked to the ability of PAA to slide along DNA; see below. In turn, PEI and PVA show intermediate behavior: the local fluctuations of the distance between the COMs of DNA and the polycation are notably smaller than those for PAA. However, there is an important difference between these two polycations with a protonation level of 50%. Visual inspection of the MD trajectories shows that a PEI chain in a complex is mainly lined up along the phosphate groups of DNA (starting from ~ 175 ns), whereas a PVA chain shows such a behavior only during the initial period of the simulations (until ~ 350 ns). At longer times, the polycation loses tight contacts with the phosphate groups of DNA and eventually gets embedded into the major groove of the DNA double helix. We note that such embedding is seen in all three simulations with PVA; see Table 1.

To further characterize the dynamic properties of DNA–polycation complexes, we focused on the time evolution of the distances between the COMs of DNA and a polycation along the DNA helical axis. As a DNA dodecamer is not a rigid helix, we utilized the following approach. We chose four DNA bases in the middle of the dodecamer (adenine, thymine, and their complementary bases) and treated them as rigid. For four atoms of the chosen bases (C5 atoms), we calculated the coefficients for the DNA helical axis equation, identifying thereby the direction of the DNA helical axis in every frame of simulations. The results are presented in Figure 3.

The position of zero on the Y axis of Figure 3 corresponds to the COM of DNA. Correspondingly, the position of the COM of the polycation along the helical axis of DNA can be characterized by either positive or negative values. Figure 3 shows that PAA can slide freely along the DNA dodecamer from one side to another, which is again a signature of weak binding of the PAA polymer due to a low protonation level. In contrast, the position of the COM of a tightly bound PLL is only able to oscillate around some constant value. The backbone chain of PLL can move with respect to its relatively long side chains, thereby leading to a rather large magnitude of oscillations; see Figure 3. Additionally, as some of the PLL side chains stay in the water phase and are not bound to DNA (see the next Section), these side chains also can contribute to the COM movement of PLL along the helical axis of DNA. As far as PEI is concerned, one can observe its slow movement along the dodecamer, accompanied by relatively small local

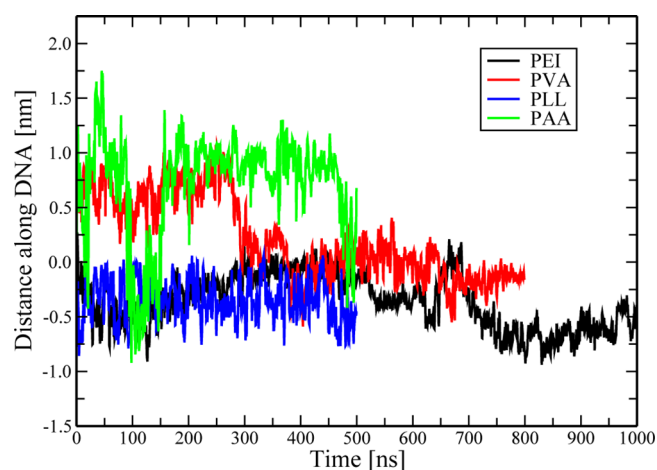


Figure 3. Time evolution of the distances between the COMs of DNA and the polymer along the DNA helix (see text for details). Results for the PEI-1 (black line), PVA-1 (red line), PAA-2 (green line), and PLL-1 (blue line) systems are shown.

fluctuations. Finally, Figure 3 shows that PVA demonstrates a similar behavior for the first 300 ns. At longer times, PVA slides to the central part of the dodecamer and stays there for the rest of the simulation run. As mentioned above, this corresponds to the embedding of PVA into the major groove of DNA.

The mobility of a polycation along the dodecamer can further be characterized through the mean-square displacement of the polycation along the helical axis of DNA. To improve the accuracy, we divided the MD trajectories for DNA–polycation systems into blocks of 10 ns and computed the mean-square displacement separately for each block. The resulting mean-square displacements averaged over full trajectories, with the exception of the first 100 ns, are shown in Figure 4. As one can

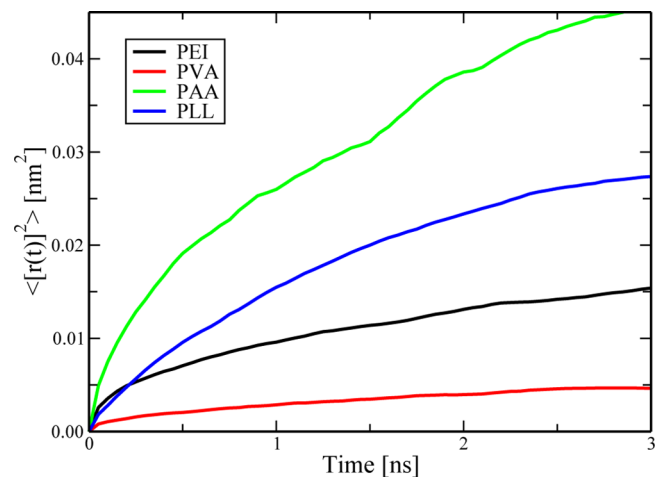


Figure 4. Mean-square displacements of the polycations along the DNA helix. Results for the PEI-1 (black line), PVA-1 (red line), PAA-2 (green line), and PLL-1 (blue line) systems are shown.

see, the mobility of PAA is the highest, in line with the conclusions made on the basis of Figure 3. PLL and PEI show some intermediate behavior. Remarkably, the mean-square displacement of PVA along the DNA is considerably smaller than that of the other polycations; see Figure 4. Therefore, one can conclude that embedding into a major groove of DNA

leads to pronounced immobilization of a polymer, most likely due to steric restrictions within the DNA groove.

Structure of DNA–Polycation Complexes. Binding of a polycation to a DNA dodecamer could potentially affect the conformation of the DNA. The initial reference structure in our study was a fragment of DNA in the canonical B-form. In a control (polycation-free) simulation of a DNA dodecamer in aqueous solution, the average root-mean-square deviation (RMSD) from the reference B-form structure was found to be 0.22 ± 0.04 nm, in agreement with ref 34. In Figure 5, we

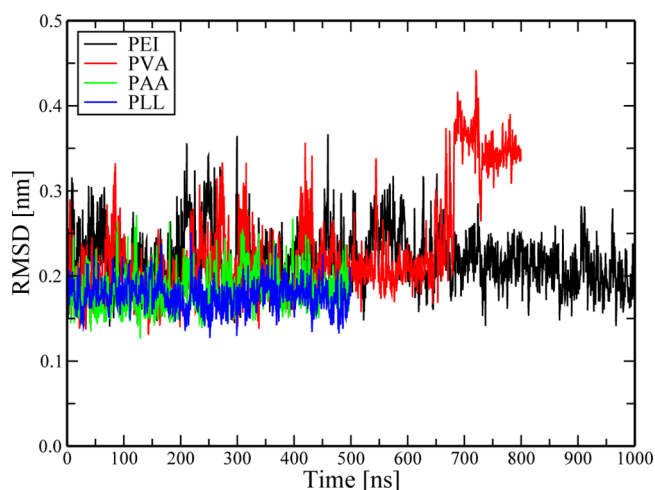


Figure 5. Time evolution of the RMSD of DNA from the reference B-form structure in a DNA–polycation complex. Results for the PEI-1 (black line), PVA-1 (red line), PAA-2 (green line), and PLL-1 (blue line) systems are shown.

show the time evolution of the RMSDs for selected DNA–polycation systems (note that two base pairs on both DNA ends were excluded from the RMSD calculations to eliminate possible end effects). As one can see, formation of a complex with a polycation does not have an impact on the secondary structure of DNA for all considered cationic polymers. In some cases (e.g., for a PLL system), the average RMSD value is even somewhat smaller than that for a pure DNA system. An increase in the RMSD at the end of a MD run for the PVA-1 system (see Figure 5) should be considered as an artifact, as it is caused by breakage of hydrogen bonds within the G–C base pair at the end of the DNA. This defect is stabilized by a tight contact formed between the unwound guanine base and a protonated amine group of PVA and propagates to a base pair next to the unwound one, giving rise to an increase in the RMSD for the PVA-1 system at $t > 700$ ns.

The radial distribution function (RDF) represents another important quantity that is able to provide insight into the structure of a DNA–polycation complex. In Figure 6 (top), we show the RDFs for nitrogen atoms of the protonated amine groups of the polycations and phosphate atoms of DNA for complexes with PEI, PLL, and PAA (the first 100 ns were excluded from each MD trajectory for RDF calculations). For all three polycations, we observe a pronounced peak in the RDF, which implies a strong electrostatic attraction between the oppositely charged amine groups of the polymer and phosphate groups of DNA. The very similar shapes and heights of the RDF peaks for different cationic polymers highlight an important role of N–P interactions in stabilizing their complexes with DNA. Besides the phosphate groups of DNA,

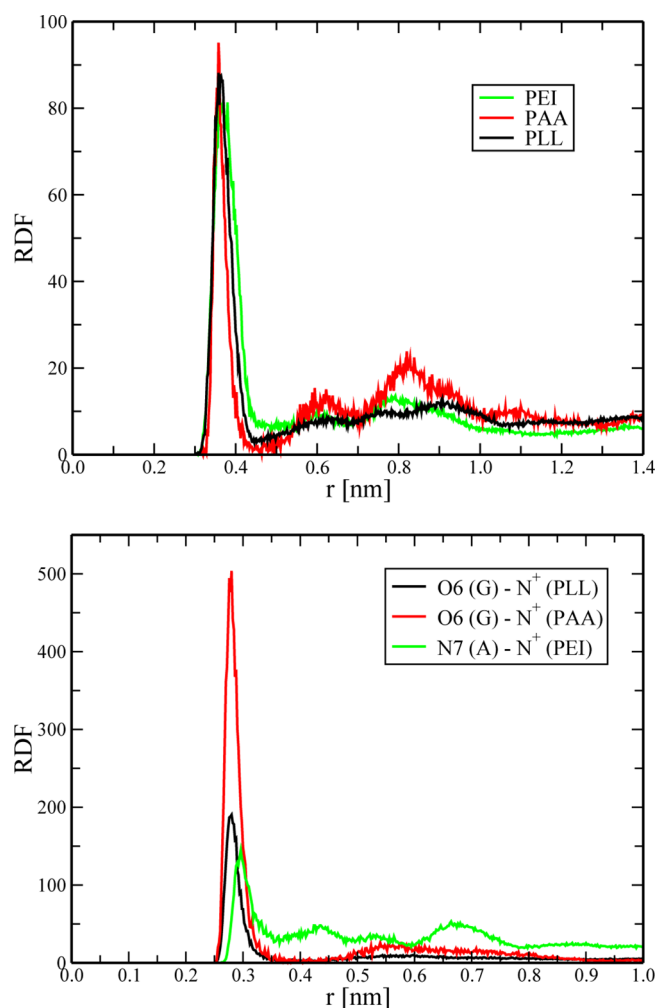


Figure 6. RDFs for nitrogen atoms of the protonated amine groups of the polymers with phosphate atoms (top) and selected electronegative atoms in the grooves (bottom) of DNA. Results for the PEI-1 (green line), PAA-2 (red line), and PLL-1 (black line) systems are shown.

the protonated amine groups of polycations also can interact favorably with some electronegative atoms in DNA grooves; see Figure S1 for the numbering of the atoms of DNA bases. In particular, one can observe pronounced RDF peaks of the amine groups with O6 oxygen atoms of guanine bases (PLL and PAA) and N7 nitrogen atoms of adenine bases (PEI); see Figure 6 (bottom) (we note that in the case of systems with PAA a pronounced RDF peak for the O6(G)–N⁺ pair is observed only for the PAA-2 system). It is noteworthy that PEI has the weakest interactions with DNA grooves (i.e., the shortest RDF peak in Figure 6 (bottom)), which is a signature of the preferential binding of PEI with the phosphate groups of DNA.

The situation for complexes of DNA with PVA is completely different. As discussed above although PVA does interact with the phosphate groups of DNA in the initial part of the trajectory, it eventually ends up in the major groove of DNA. This can directly be seen by inspecting the RDFs between protonated amine groups of PVA and phosphate groups of DNA, which are calculated over different time intervals; see Figure 7. In the initial part of the MD trajectory (200–400 ns), one can see a pronounced RDF peak similar to that for the rest of the cationic polymers; see Figure 6. However, at longer times

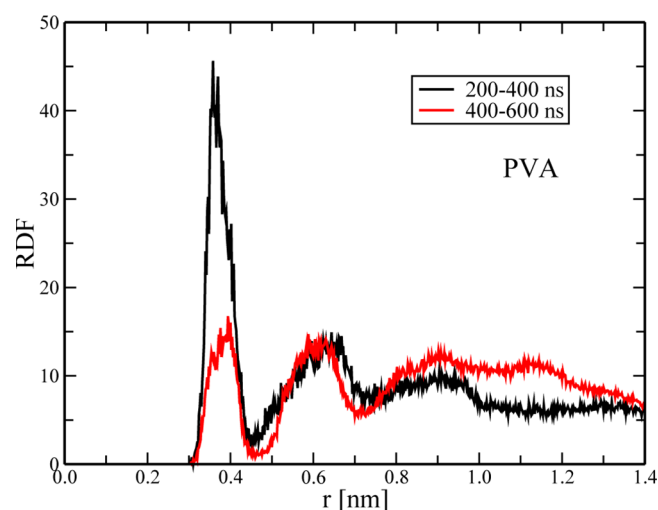


Figure 7. RDFs of nitrogen atoms of the protonated amine groups of PVA with phosphate atoms of DNA. Results averaged over different periods of MD simulations of the PVA-1 system are shown: 200–400 ns (black line) and 400–600 ns (red line).

(400–600 ns), PVA leaves the phosphate groups and gets embedded into the major groove of DNA; hence, the corresponding RDF peak disappears. Such embedding into the DNA groove should also be observed in the RDFs of the amine groups of PVA with selected atoms of the major groove. Indeed, Figure 8 confirms that the corresponding RDFs are sensitive to the time interval used for calculating the RDFs. All in all, we found that the protonated amine groups of PVA interact mostly with N7 nitrogen atoms and O6 oxygen atoms of guanine bases and O4 oxygen atoms of thymine bases in a DNA groove. In the time interval from 200 to 400 ns, the amine groups of PVA interact preferably with the phosphate groups of DNA; hence, the RDFs in Figure 8 (top) are characterized by relatively small first peaks. However, when PVA is embedded into the DNA groove, the peaks become much higher and more pronounced, indicating thereby stronger interactions between the polymer and major groove of DNA. It should also be noted that all of the mentioned atoms in the groove have a relatively large negative charge (approximately $-0.55e$ each); hence, electrostatic attraction should play a certain role in the embedding of PVA into the major groove.

Another interesting aspect of a DNA–polycation complex is the effect of polymer geometry on the size of the complex. Inspection of Figures 6 (top) and 7 shows that the positions of RDF peaks for protonated amine groups and phosphate groups of DNA coincide for all four polycations so that steric effects due to differences in chain geometry do not have an impact on the binding distance between the protonated polymer groups and DNA. Therefore, all of the differences in binding that are observed for the COMs of the polymers and DNA (see Figure 2) can directly be linked to polymer geometry. Averaging of these distances over MD trajectories (with the exception of the first 100 ns) gives 0.5 ± 0.2 , 0.8 ± 0.2 , 1.1 ± 0.2 , and 1.3 ± 0.1 nm for PEI, PVA, PAA, and PLL, respectively. Remarkably, there is a direct relation of the compactness of a DNA–polycation complex with the length of the side chains; see Figure 1: the shorter the side chains, the more compact the complex. We also note that as far as DNA complexes with PEI and PLL are concerned, this finding is in qualitative agreement with that of an earlier computational study.¹⁸

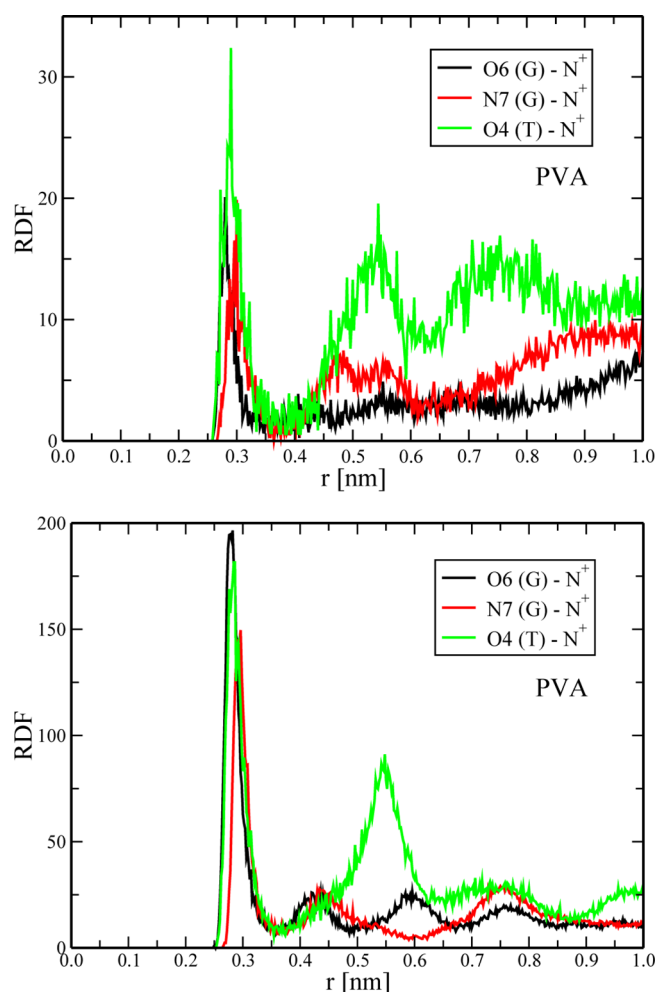


Figure 8. RDFs of nitrogen atoms of the protonated amine groups of PVA with selected electronegative atoms in the DNA grooves. Results averaged over different periods of MD simulations of the PVA-1 system are shown: 200–400 ns (top) and 400–600 ns (bottom).

Finally, we considered the time evolution of the number of contacts between the protonated amine groups of polycations and the phosphate groups of DNA. The calculations were performed in line with ref 46. First, we calculated the corresponding RDFs and identified the radii of the first coordination shells (defined as positions of the first RDF minima). The number of contacts was then calculated by counting the number of appropriate atoms within the first coordination sphere. The corresponding numbers of contacts for selected systems are shown in Figure 9.

The first interesting feature of Figure 9 is the fact that the number of N–P contacts for PEI slightly exceeds the corresponding quantity for PLL (we recall that the total number of protonated amine groups of PLL is 2 times larger than that for PEI). This can be explained by the flexible nature of PEI because of which it can line up along many phosphate groups of DNA. In contrast, PLL is a bulky polymer with a relatively high linear charge density; hence, many of its side chains cannot access DNA phosphates and stay in aqueous solution.

The very small number of P–N contacts for PAA is due to the small overall charge of the polymer ($+4e$). In contrast, the total charge of PVA is the same as that for PEI. However, we observe a considerably smaller number of P–N contacts in the

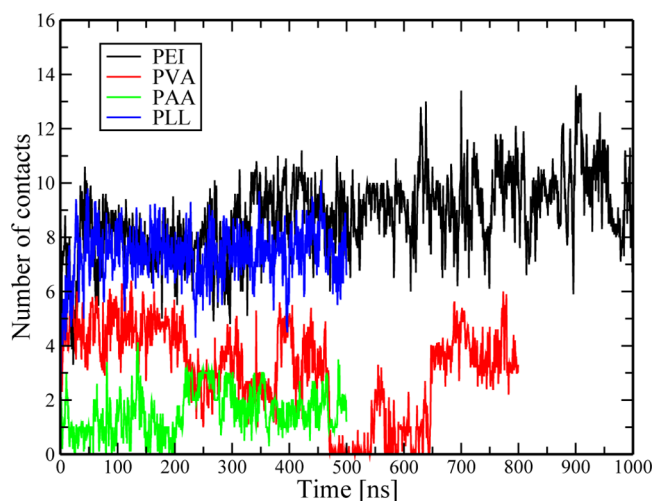


Figure 9. Number of contacts of protonated amine groups of polycations with phosphate groups of DNA. Results for the PEI-1 (black line), PVA-1 (red line), PAA-2 (green line), and PLL-1 (blue line) systems are shown.

case of PVA due to the above-mentioned embedding of the polymer into the major groove; see Figure 9. This is particularly pronounced in the time interval from 450 to 650 ns during which one can observe even a complete loss of P–N contacts; hence, only interactions between the polymer and major groove of DNA are responsible for the stability of the complex. We note that such a behavior was witnessed for all three PVA systems; see Table 1.

DISCUSSION AND CONCLUSIONS

As synthetic cationic polymers represent a promising class of delivery vectors for gene therapy, in this study we employed atomistic MD simulations to get a molecular-level insight into the structure and properties of complexes of DNA with various polycations. We considered cationic polymers with two different types of backbone chains. The first type of polymers (PEI and PLL) is characterized by the presence of amine groups in their backbone chains. Polymers of the second type (PVA and PAA) have a hydrocarbon main chain. It should be stressed that our work is the first in which complexes of DNA with PVA and PAA were studied using atomic-scale MD simulations. It is noteworthy that the differences in the chemical structure of these four polycations (see Figure 1) are not only in the polymer geometry but also in the protonation state. In particular, under physiologic conditions, the protonation levels of PEI, PLL, PVA, and PAA were 50, 100, 50, and 20%, respectively, in line with the experimental data available.

Overall, for all of the polycations in question, the initial formation of a complex with DNA is driven by the electrostatic attraction between the protonated amine groups of the polycation and phosphate groups of DNA (N–P contacts). This is in line with earlier MD studies of complexes of DNA with polycations.^{15,18,21,24,25} The stability of the resulting complexes in terms of the overall number of N–P contacts depends on both the protonation state and the polymer topology. In particular, it comes as no surprise that PAA, carrying the lowest charge among the polymers, forms the weakest complex with DNA. In turn, complexes of DNA with PLL and PEI are found to be characterized by approximately

the same numbers of N–P contacts, despite the fact that the overall charge of PLL is 2 times larger than that of PEI. This is most likely because of the geometrical differences in these polymers. PEI is a linear flexible polymer that is able to line up along the phosphate groups of DNA. In contrast, PLL is rather bulky; hence, some of its side chains cannot access the negative charges of DNA.

Interestingly, the above binding pattern of N–P contacts stays unchanged in complexes of DNA with PEI, PLL, and PAA. However, PVA demonstrates an alternative pattern of binding to DNA: after an initial period of relatively stable N–P contacts, the polymer gets embedded into the major groove of DNA, thereby leaving the phosphate groups of DNA; see Figure 10. We found that the protonated amine groups of PVA

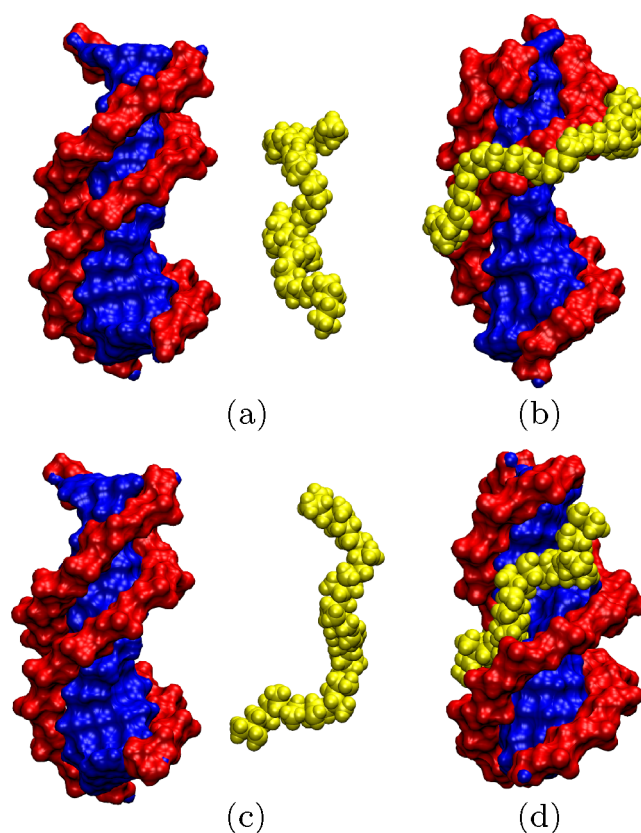


Figure 10. Snapshots of the initial and final structures of DNA–polycation complexes for the PEI-1 system ($t = 0$ ns (a) and $t = 1$ μ s (b)) and PVA-1 system ($t = 0$ ns (c) and $t = 650$ ns (d)). Visualization is made using the VMD package.⁴⁷

interact favorably with several electronegative atoms of the major groove after embedding. To the best of our knowledge, such a pattern of binding of a polycation to DNA is reported here for the first time.

In general, one can think of two possible factors that could potentially lead to the embedding of a polycation into the DNA major groove. First is the affinity of the backbone chain of the polymer to the DNA groove. PVA has a hydrocarbon main chain that is more hydrophobic than that of PLL and PEI; this hydrophobicity could promote embedding of PVA into the groove. However, such an effect is not observed in the case of PAA, another polycation with a hydrocarbon backbone chain. One could argue that PAA is not able to form stable complexes with DNA due to its small overall charge. To gain insight into

the role of the protonation level, we increased the PAA protonation to 50% (the same level as that for PVA) and performed a series of additional simulations; see Table 1. It turned out that PAA still showed only a binding pattern related to N–P contacts, and no polymer embedding into the major groove was observed. This implies that besides the hydrophobicity of the backbone chain, the overall polymer geometry also plays a crucial role: as PVA has small side chains (they are shorter than those of PAA), it could better fit into the major groove of DNA.

The striking difference in binding patterns that is found for PEI and PVA, two polymers of the same protonation level (Figure 10), has some important biomedical implications. As complexes of DNA and PEI are governed mainly by N–P contacts, they should be much more sensitive to changes in the aqueous environment compared to complexes with PVA (pH level, salt ions, etc.). To explore this, we carried out two additional simulations of stable complexes of DNA with PEI and PVA in the presence of 1 M CaCl₂ salt; see Table 1. Such a high salt concentration should screen effectively the electrostatic interactions between charged residues of DNA and polycations, thereby weakening their binding. In both cases, we were unable to observe complete decomplexation during 700 ns; for PEI (protonation level 50%), this conclusion is in line with the findings of an earlier study.²³ However, we found that adding a divalent salt differently affects the average number of contacts between the phosphate groups of DNA and protonated amine groups for the two polymers: 6.2 ± 2.0 (8.9 ± 1.6) for PEI versus 2.2 ± 1.1 (2.8 ± 1.8) for PVA for systems with (without) a divalent salt. Therefore, it is seen that the response of a PVA–DNA complex to salt ions is indeed much weaker compared to that of a DNA complex with PEI, a linear cationic polymer of the same protonation level.

The fact that PVA responds only weakly to the changes in aqueous solution implies that the intracellular release of genetic material from a delivery vector could be considerably hindered, leading to insufficient gene expression and correspondingly to lower transfection activity. Remarkably, this theoretical prediction is in line with the experimental results: it was indeed shown that the transfection activity of PVA is much lower than that observed, for example, for PAA.²⁷ Therefore, our study provides a molecular-level basis for the above experimental finding.

■ ASSOCIATED CONTENT

■ Supporting Information

The Supporting Information is available free of charge on the ACS Publications website at DOI: 10.1021/acs.jpcb.6b03779.

Numbering of atoms of DNA bases, distribution of protonated and deprotonated monomers in cationic polymers, atom types, and partial charges of polymer atoms in a schematic representation and the Gromacs topology format (PDF)

■ AUTHOR INFORMATION

Corresponding Author

*E-mail: agurtovenko@gmail.com. Phone: +7-812-3285601. Fax: +7-812-3286869. Website: biosimu.org.

Notes

The authors declare no competing financial interest.

■ ACKNOWLEDGMENTS

The authors wish to acknowledge the use of the computer cluster of the Institute of Macromolecular Compounds RAS and the Lomonosov supercomputer at the Moscow State University. This work was supported by the Russian Foundation of Basic Research through Grant No. 14-03-01073.

■ REFERENCES

- (1) Samal, S. K.; Dash, M.; van Vlierberghe, S.; Kaplan, D. L.; Chiellini, E.; van Blitterswijk, C.; Moroni, L.; Dubruel, P. Cationic polymers and their therapeutic potential. *Chem. Soc. Rev.* **2012**, *41*, 7147–7194.
- (2) Zhang, X. J.; Godbey, W. T. Viral vectors for gene delivery in tissue engineering. *Adv. Drug Delivery Rev.* **2006**, *58*, 515–534.
- (3) Lehrman, S. Virus treatment questioned after gene therapy death. *Nature* **1999**, *401*, 517–518.
- (4) Oupicky, D.; Konak, C.; Ulbrich, K.; Wolfert, M. A.; Seymour, L. W. DNA delivery systems based on complexes of DNA with synthetic polycations and their copolymers. *J. Controlled Release* **2000**, *65*, 149–171.
- (5) Luten, J.; van Nostrum, C. F.; Smedt, S. C. D.; Hennink, W. E. Biodegradable polymers as non-viral carriers for plasmid DNA delivery. *J. Controlled Release* **2008**, *126*, 97–110.
- (6) Spizizen, J.; Reilly, B.; Evans, A. Microbial transformation and transfection. *Annu. Rev. Microbiol.* **1966**, *20*, 371–400.
- (7) Bergstrand, A.; Rahmani-Monfared, G.; Ostlund, A.; Nyden, M.; Holmberg, K. Comparison of PEI-PEG and PLL-PEG copolymer coatings on the prevention of protein fouling. *J. Biomed. Mater. Res., Part A* **2009**, *88A*, 608–615.
- (8) Yu, H. J.; Deng, C.; Tian, H. Y.; Lu, T. C.; Chen, X. S.; Jing, X. B. Chemo-physical and biological evaluation of poly(L-lysine)-grafted chitosan copolymers used for highly efficient gene delivery. *Macromol. Biosci.* **2011**, *11*, 352–361.
- (9) Boussif, O.; Ezoulach, F.; Zanta, M. A.; Mergny, M. D.; Scherman, D.; Demeneix, B.; Behr, J. P. A versatile vector for gene and oligonucleotide transfer into cells in culture and in vivo: polyethylenimine. *Proc. Natl. Acad. Sci. U.S.A.* **1995**, *92*, 7297–7301.
- (10) Godbey, W. T.; Wu, K. K.; Mikos, A. Poly(ethylenimine)-mediated gene delivery affects endothelial cell function and viability. *Biomaterials* **2001**, *22*, 471–480.
- (11) Tay, C. Y.; Menon, N.; Leong, D. T.; Tan, L. P. Molecular architecture governs cytotoxicity and gene transfection efficacy of polyethylenimine based nanoplexes in mammalian cell lines. *J. Inorg. Organomet. Polym.* **2015**, *25*, 301–311.
- (12) Petersen, H.; Martin, A. L.; Stolnik, S.; Roberts, C. J.; Davies, M. C.; Kissel, T. The macrostopper route: a new synthesis concept leading exclusively to diblock copolymers with enhanced DNA condensation potential. *Biomacromolecules* **2002**, *35*, 9854–9856.
- (13) Ihm, J. E.; Krier, I.; Lim, J. M.; Shim, S.; Han, D. K.; Hubbell, J. A. Improved biocompatibility of polyethylenimine (PEI) as a gene carrier by conjugating urocanic acid: in vitro and in vivo. *Macromol. Res.* **2015**, *23*, 387–395.
- (14) Park, E.; Cho, H.-B.; Takimoto, K. Effective gene delivery into adipose-derived stem cells: transfection of cells in suspension with the use of a nuclear localization signal peptide-conjugated polyethylenimine. *Cytotherapy* **2015**, *17*, 536–542.
- (15) Meneksedag-Erol, D.; Tang, T.; Uludag, H. Molecular modeling of polynucleotide complexes. *Biomaterials* **2014**, *35*, 7068–7076.
- (16) Korolev, N.; Lyubartsev, A. P.; Laaksonen, A.; Nordenskiöld, L. On the competition between water, sodium ions, and spermine in binding to DNA: a molecular dynamics computer simulation study. *Biophys. J.* **2002**, *82*, 2860–2875.
- (17) Korolev, N.; Lyubartsev, A. P.; Laaksonen, A.; Nordenskiöld, L. A molecular dynamics simulation study of oriented DNA with polyamine and sodium counterions: diffusion and averaged binding of water and cations. *Nucleic Acids Res.* **2003**, *31*, 5971–5981.
- (18) Ziebarth, J.; Wang, Y. M. Molecular dynamics simulations of DNA-polycation complex formation. *Biophys. J.* **2009**, *97*, 1971–1983.

- (19) Ouyang, D.; Zhang, H.; Herten, D. P.; Parekh, H. S.; Smith, S. C. Structure, dynamics, and energetics of siRNA-cationic vector complexation: a molecular dynamics study. *J. Phys. Chem. B* **2010**, *114*, 9220–9230.
- (20) Ouyang, D.; Zhang, H.; Parekh, H. S.; Smith, S. C. Structure and dynamics of multiple cationic vectors-siRNA complexation by all-atomic molecular dynamics simulations. *J. Phys. Chem. B* **2010**, *114*, 9231–9237.
- (21) Elder, R. M.; Emrick, T.; Jayaraman, A. Understanding the effect of polylysine architecture on DNA binding using molecular dynamics simulations. *Biomacromolecules* **2011**, *12*, 3870–3879.
- (22) Antila, H. S.; Sammalkorpi, M. Polyelectrolyte decomplexation via addition of salt: charge correlation driven zipper. *J. Phys. Chem. B* **2014**, *118*, 3226–3234.
- (23) Antila, H. S.; Harkonen, M.; Sammalkorpi, M. Chemistry specificity of DNA-polycation complex salt response: a simulation study of DNA, polylysine and polyethyleneimine. *Phys. Chem. Chem. Phys.* **2015**, *17*, 5279–5289.
- (24) Sun, C. B.; Tang, T.; Uludag, H.; Cuervo, J. E. Molecular dynamics simulations of DNA/PEI complexes: effect of PEI branching and protonation state. *Biophys. J.* **2011**, *100*, 2754–2763.
- (25) Sun, C.; Tang, T.; Uludag, H. Molecular dynamics simulations for complexation of DNA with 2 kDa PEI reveal profound effect of PEI architecture on complexation. *J. Phys. Chem. B* **2012**, *116*, 2405–2413.
- (26) Wolfert, M. A.; Dash, P. R.; Nazarova, O.; Oupicky, D.; Seymour, L. W.; Smart, S.; Strohm, J.; Ulbrich, K. Polyelectrolyte vectors for gene delivery: influence of cationic polymer on biophysical properties of complexes formed with DNA. *Bioconjugate Chem.* **1999**, *10*, 993–1004.
- (27) Slita, A. V.; Kasyanenko, N. A.; Nazarova, O. V.; Gavrilova, I. I.; Eropkina, E. M.; Sirotkin, A. K.; Smirnova, T. D.; Kiselev, O. I.; Panarin, E. F. DNA-polycation complexes - effect of polycation structure on physico-chemical and biological properties. *J. Biotechnol.* **2007**, *127*, 679–693.
- (28) Drew, H. R.; Dickerson, R. E. Structure of a B-DNA dodecamer. III. Geometry of hydration. *J. Mol. Biol.* **1981**, *151*, 535–556.
- (29) Dickerson, R. E.; Ng, H. L. DNA structure from A to B. *Proc. Natl. Acad. Sci. U.S.A.* **2001**, *98*, 6986–6988.
- (30) Antipina, A. Yu; Gurtovenko, A. A. Molecular-level insight into the interactions of DNA with phospholipid bilayers: barriers and triggers. *RSC Adv.* **2016**, *6*, 36425–36432.
- (31) Suh, J.; Paik, H. J.; Hwang, B. K. Ionization of poly(ethylenimine) and poly(allylamine) at various pHs. *Bioorg. Chem.* **1994**, *23*, 318–327.
- (32) Smits, R. G.; Koper, G. J. M.; Mandel, M. The influence of nearest-neighbor and next-nearest-neighbor interactions on the potentiometric titration of linear poly(ethylenimine). *J. Phys. Chem.* **1993**, *97*, 5745–5751.
- (33) Katchalsky, A.; Mazur, J.; Spitnik, P. Polybase properties of polyvinylamine. *J. Polym. Sci.* **1957**, *23*, 513–532.
- (34) Perez, A.; Marchan, I.; Svozil, D.; Spomer, J.; Cheatham, T. E.; Loughton, C. A.; Orozco, M. Refinement of the AMBER force field for nucleic acids: improving the description of alpha/gamma conformers. *Biophys. J.* **2007**, *92*, 3817–3829.
- (35) Wang, J. M.; Cieplak, P.; Kollman, P. A. How well does a Restrained Electrostatic Potential (RESP) model perform in calculating conformational energies of organic and biological molecules? *J. Comput. Chem.* **2000**, *21*, 1049–1074.
- (36) Jorgensen, W. L.; Chandrasekhar, J.; Madura, J. D.; Impey, R. W.; Klein, M. L. Comparison of simple potential functions for simulating liquid water. *J. Chem. Phys.* **1983**, *79*, 926–935.
- (37) Joung, I. S.; Cheatham, T. E. Determination of alkali and halide monovalent ion parameters for use in explicitly solvated biomolecular simulations. *J. Phys. Chem. B* **2008**, *112*, 9020–9041.
- (38) Stevens, W. J.; Basch, H.; Krauss, M. Compact effective potentials and efficient shared-exponent basis sets for the first- and second-row atoms. *J. Chem. Phys.* **1984**, *81*, 6026.
- (39) Granovsky, A. A. *Firefly* version 8, 2007.
- (40) Wang, J.; Wolf, R. M.; Caldwell, J. W.; Kollman, P. A.; Case, D. A. Development and testing of a general amber force field. *J. Comput. Chem.* **2004**, *25*, 1157–1174.
- (41) Bayly, C. I.; Cieplak, P.; Cornell, W.; Kollman, P. A. A well-behaved electrostatic potential based method using charge restraints for deriving atomic charges: the RESP model. *J. Phys. Chem.* **1993**, *97*, 10269–10280.
- (42) Bussi, G.; Donadio, D.; Parrinello, M. Canonical sampling through velocity rescaling. *J. Chem. Phys.* **2007**, *126*, 014101.
- (43) Parrinello, M.; Rahman, A. Polymorphic transitions in single crystals: a new molecular dynamics method. *J. Appl. Phys.* **1981**, *52*, 7182–7190.
- (44) Essman, U.; Perera, L.; Berkowitz, M.; Darden, T.; Lee, H.; Pedersen, L. G. A smooth particle mesh Ewald method. *J. Chem. Phys.* **1995**, *103*, 8577–8592.
- (45) Hess, B.; Kutzner, C.; van der Spoel, D.; Lindahl, E. GROMACS 4: algorithms for highly efficient, load-balanced and scalable molecular simulation. *J. Chem. Theory Comput.* **2008**, *4*, 435–447.
- (46) Gurtovenko, A. A.; Vattulainen, I. Effect of NaCl and KCl on phosphatidylcholine and phosphatidylethanolamine lipid membranes: insight from atomic-scale simulations for understanding salt-induced effects in the plasma membrane. *J. Phys. Chem. B* **2008**, *112*, 1953–1962.
- (47) Humphrey, W.; Dalke, A.; Schulten, K. VMD: visual molecular dynamics. *J. Mol. Graphics* **1996**, *14*, 33–38.